# Dynamical effects and intermediate mass fragment production in peripheral and semicentral collisions of Xe+Sn at 50 MeV/nucleon

J. Łukasik,[1,*] J. Benlliure,[2] V. Métivier,[3,†] E. Plagnol,[1] B. Tamain,[3] M. Assenard,[6] G. Auger,[2] Ch. O. Bacri,[1] E. Bisquer,[4] B. Borderie,[1] R. Bougault,[3] R. Brou,[3] Ph. Buchet,[5] J. L. Charvet,[5] A. Chbihi,[2] J. Colin,[3] D. Cussol,[3] R. Dayras,[5] A. Demeyer,[4] D. Doré,[1] D. Durand,[3] E. Gerlic,[4] S. Germain,[6] D. Gourio,[6] D. Guinet,[4] P. Lautesse,[4] J. L. Laville,[6] J. F. Lecolley,[3] A. Le Fèvre,[2] T. Lefort,[3] R. Legrain,[5] O. Lopez,[3] M. Louvel,[3] N. Marie,[2] L. Nalpas,[5] M. Parlog,[1,‡] J. Péter,[3] O. Politi,[2] A. Rahmani,[6] T. Reposeur,[6] M. F. Rivet,[1] E. Rosato,[3] F. Saint-Laurent,[2] M. Squalli,[1] J. C. Steckmeyer,[3] M. Stern,[4] L. Tassan-Got,[1] E. Vient,[3] C. Volant,[5] J. P. Wieleczko,[2] M. Colonna,[5] F. Haddad,[6] Ph. Eudes,[6] T. Sami,[6] and F. Sebille[6]

[1]*IPN, IN2P3-CNRS, F-91406 Orsay Cedex, France*

[2]*GANIL, CEA, IN2P3-CNRS, B.P. 5027, F-14021 Caen Cedex, France*

[3]*LPC, IN2P3-CNRS, ISMRA et Université, F-14050 Caen Cedex, France*

[4]*IPN Lyon, IN2P3-CNRS et Université, F-69622 Villeurbanne Cedex, France*

[5]*CEA, DAPNIA/SPhN, CEN Saclay, F-91191 Gif sur Yvette Cedex, France*

[6]*SUBATECH, IN2P3-CNRS/EMN/Université, F-44070 Nantes Cedex 03, France*

(Received 6 November 1996)

Experimental data obtained with the $4\pi$ multidetector system INDRA are used to study the light charged particle (LCP, $Z \leqslant 2$) and intermediate mass fragment (IMF, $Z \geqslant 3$) production in peripheral and semicentral collisions of Xe and Sn at 50 MeV/nucleon. It is found that a sizable fraction of the detected LCP's and IMF's originates from the midvelocity region. These fragments can be seen to come either from a prompt (preequilibrium) mechanism or from a slower but dynamically influenced emission process. The relative magnitude of the dynamically influenced emission relative to the isotropic statistical evaporation is presented as a function of the transverse energy of light particles, used as an impact parameter selector. The results are compared to dynamical models with which a good agreement is obtained. [S0556-2813(97)04203-9]

PACS number(s): 25.70.Mn, 25.70.Lm, 25.70.Pq

## I. INTRODUCTION

The understanding of dynamical effects which lead to dissipation of energy in heavy-ion collisions in the intermediate energy range (20–100 MeV/nucleon) has been a goal of many studies because they reflect intrinsic properties of nuclear matter. Recent experimental studies [1–5], the results of which are in agreement with theoretical calculations [6,7], have demonstrated that for most collisions (from peripheral to almost central), the mechanisms are mainly binary. This feature can be compared with the corresponding behavior at lower and higher bombarding energies. Below 10 MeV/nucleon, binary processes, deep inelastic collisions (DIC), are indeed widely observed, mainly for heavy systems. The reaction is purely binary in the sense that it leads to two excited outgoing products which deexcite by sequential binary decays. In relativistic heavy-ion collisions a third emitting source is observed, which is labeled a ''participant zone.'' Of course one may expect a continuous evolution from a pure two-source DIC picture to this three-source picture, when the bombarding energy evolves in the intermediate energy range. However, the nature of this transition has never been studied.

The advent of large acceptance detectors has produced a wide body of data on the deviation from the purely binary picture. Several studies [8,9] have shown that, above 12 MeV/nucleon, sequential fission events for a medium size system point to a very fast process where the fission products are often aligned along the deflection axis and are not isotropically distributed as they should be if long fission lifetimes were assumed. For higher energies and various systems, a number of groups [10–18] have shown that, for peripheral reactions, some fraction of the intermediate mass fragments (IMF's) comes from the region in velocity space that could imply the emission of fast dynamical particles and fragments or the formation of a ''neck.''

A number of effects could explain the presence of particles with velocities intermediate between the apparent quasiprojectile (QP) and quasitarget (QT) velocities.

First and foremost, the contact region between the two interacting nuclei is the obvious source of preequilibrium emissions. These, early emitted, ''prompt'' particles are those that have suffered elastic nucleon-nucleon (target-projectile) collisions which have pushed them ''outside'' the attractive potential of the bulk. For symmetric systems, the mean velocities of these particles will coincide with the total center-of-mass velocity. As defined, these particles should essentially include protons and neutrons: It is not yet understood to what extent more complex fragments (e.g., $\alpha$ particles) could be emitted in this manner.

*Permanent address: Institute of Nuclear Physics, ul. Radzikowskiego 152, PL-31-342 Kraków, Poland.

†Present address: SUBATECH, IN2P3-CNRS/Université/EMN, F-44070 Nantes Cedex 03, France.

‡Permanent address: Institute of Physics and Nuclear Engineering, IFA, P.O. Box MG6, Bucharest, Romania.

 

More collectively and depending whether the interacting nuclei make contact for sufficient time, a neck of matter may join them and, unless fusion follows, the size and breaking of this neck will depend on the impact parameter as well as on the relative velocity. It must be noted that although a neck of matter may be defined, it does not follow that complete stopping of the two nuclei is achieved. On the contrary, the existence of a neck can be seen as that part of matter which participates in the collision process whereas the remaining mass continues unhampered in its trajectory. In this case, the neck could be viewed as a ''hot spot'' whose temperature may be significantly different from the rest of the matter: This is the underlying assumption of the ''participant-spectator'' scenario.

Following what is observed in the collision of viscous liquid droplets [19], a number of complex scenarios can be imagined: The breaking of the neck can take place at its waist and leave the two nuclei in a deformed configuration. This may be followed either by the emission of this ''deformation'' zone and could be termed as a dynamically induced fission or by the absorption of this deformation and subsequent statistical cooling. A scenario very similar to this one would correspond to the asymmetric breaking of the neck, leaving most of the neck matter on one of the participating nuclei. In the case of dynamical fission, the velocities expected for the emitted fragment(s) would correspond to values intermediate between those of the QT and QP, and presumably closer to one than to the other depending on the rapidity of the process. Coulomb repulsion energies could thus be observed for these processes. Angular momentum effects may also influence the velocity and angular distributions and different situations may be encountered depending on the duration of the fission process relative to the rotational period.

Another scenario could correspond to the shearing off of this neck from both nuclei, leaving this matter as a presumably hot third source. This would correspond to the participant zone well established at high energies. At the energies considered here, the decay of this hot matter would probably result in the presence of particle or light fragments with velocities centered on the center-of-mass velocity.

The confirmation of these various scenarios relies, in part, on the possibility to measure the ''size'' of the neck as well as the distribution of velocities of the emitted particles and fragments. This can be done with the use of efficient $4\pi$ detectors which allow almost complete mapping, event by event, of the velocity distribution of the particles and fragments as well as a reliable estimate of the impact parameter.

This paper presents the results obtained in the study of the Xe+Sn reaction at 50 MeV/nucleon using the INDRA detector. Following a brief description of the experimental conditions (Sec. II), the impact parameter selector used in this analysis will be presented (Sec. III). Section IV will show the evidence for this neck emission and Sec. V will present a quantitative estimate of these effects. Section VI will present dynamical calculations that support our interpretation of the data and conclusions will be drawn in Sec. VII.

## II. EXPERIMENTAL CONDITIONS

The experiment was performed at the GANIL accelerator with the INDRA detector. The detector can be schematically described as a set of 17 detection rings centered on the beam axis. The most forward ring ($2° \leqslant \theta_{lab} \leqslant 3°$) is made of phoswich detectors [NE102 (0.5 mm) + NE115 (25 cm)]. From 3° to 45°, eight rings are made of three detection layers (ionization chambers (5 cm of $C_3F_8$ at 30 mbar), silicon (300 $\mu$m) and CsI(Tl) [13.8–9 cm]). Beyond 45°, the remaining eight rings have double detection layers (ionization chambers [5 cm of $C_3F_8$ at 20 mbar and CsI(Tl) (7.6–5 cm)]). The total number of detection cells is 336. In the forward region ($3° \leqslant \theta_{lab} \leqslant 45°$), ions with $Z$ up to 54 are identified if their energies are greater than the Bragg peak value. Below this energy, only a minimum $Z$ value can be attributed. Beyond 45°, a proper identification is obtained up to $Z=16$, and beyond the uncertainty is estimated to be of the order of 2–3 units. Over the entire angular range, a very good isotope identification is obtained for $Z=1-3$, except for particles with low laboratory energies where ambiguities are unresolved. Computer simulations of both the detector efficiency as well as the identification and energy calibration processes show that a good understanding of the functioning of the detector is achieved. A complete technical description of the detector and of its electronics can be found in [20].

In order for the detector to function in the best conditions and to keep random coincidences down, a beam current of $5.0\times10^7$ incident Xe ions per second was used. The target was made of natural Sn with a thickness of 350 $\mu g/cm^2$. A minimal bias trigger was used that registered all the events with at least four detectors fired. The random coincidence probability is estimated to be below $10^{-4}$.

## III. IMPACT PARAMETER SELECTOR

It is a well-known fact, illustrated by dynamical calculations, that the reaction mechanism (i.e., dissipation, spin, mass, charge transfer, etc.) is very dependent on the impact parameter of the collision. Even with sophisticated $4\pi$ devices the impact parameter cannot be directly measured and an event selector, based on observed quantities, has to be defined and adapted to the detector setup. One of the properties of the INDRA detector [20] is its high efficiency (about 90%) for light charged particles (LCP's, $Z=1,2$), independently of the type of the reaction mechanism involved and of the impact parameter. Hence we use as a sorting parameter the transverse kinetic energy, $E_{trans12}$, of LCP's, defined as

$$E_{trans12}=\sum_{Z=1,2}\frac{p_\perp^2}{2m},$$

where the summation is taken over the particles with $Z=1$ or 2 only, and $p_\perp$ and $m$ are the linear momentum component perpendicular to the beam axis and mass of each of these particles, respectively. An advantage of this method is that it eliminates efficiency problems for peripheral collisions for which the projectilelike (PLF) or targetlike (TLF) fragments can be undetected due to the energy threshold (targetlike) or angular efficiency (projectilelike) effects. $E_{trans12}$ is therefore used to sort all the events registered by INDRA, without any *a priori* selection.

In Fig. 1, we present some features of $E_{trans12}$. The upper left panel presents a distribution of this observable. This

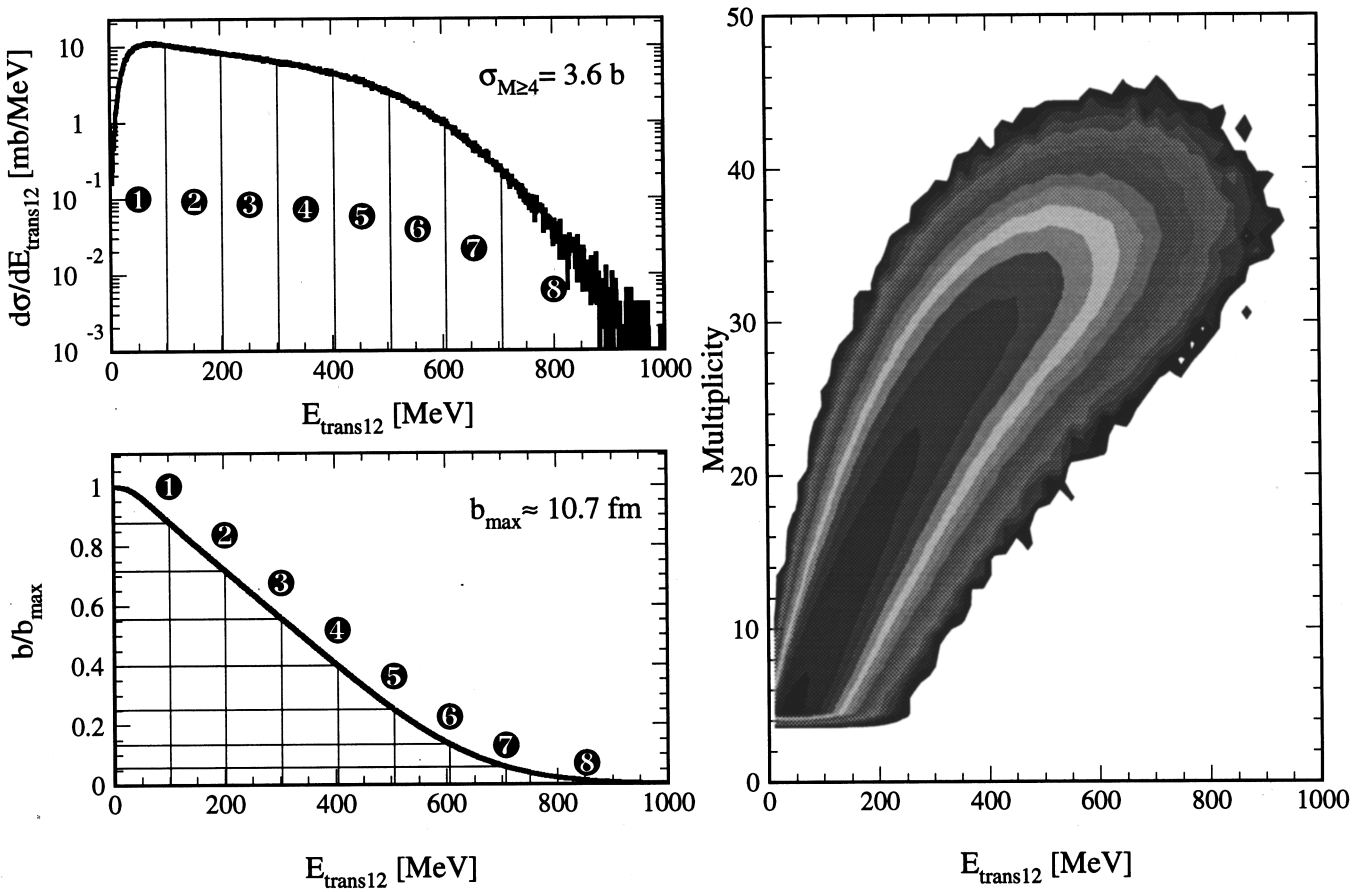


FIG. 1. Upper left panel: spectrum of the transverse energy, $E_{trans12}$, of $Z=1$ and $Z=2$ particles. Lower left panel: relation between the reduced impact parameter and $E_{trans12}$. Right panel: correlation between the multiplicity of charged particles and fragments and $E_{trans12}$. The numbers associated with the $E_{trans12}$ bins (or the impact parameter bins) are used to identify these bins in the following presentation. See text for the definition of $b_{max}$.

spectrum was divided into eight bins. The lower left panel presents the relation between $E_{trans12}$ and the reduced impact parameter, $b/b_{max}$, obtained with the use of the geometrical prescription [21]. The measured maximal impact parameter $b_{max}$ is determined by an off-line analysis threshold and refers to the events with at least four charged particles or fragments detected. This threshold was set in order to restore the original experimental trigger condition, and thus to reject the events detected with unreliable intensity. The corresponding total measured cross section $\sigma_{M\geq 4}=3.6$ b. This value of cross section allows us to estimate the value of $b_{max}$ to be about 10.7 fm. The last bin corresponds to 5% of the maximal reduced impact parameter. Nevertheless, in this study we concentrate on the peripheral and semicentral collisions (bins 1–5) which exhaust about (80–90)% of the total measured cross section. The right panel of Fig. 1, presents the correlation between $E_{trans12}$ and the total multiplicity of charged particles and fragments. The following results are presented as a function of the bin numbers defined in the left part of the figure.

## IV. VELOCITY DISTRIBUTIONS: A SIGNATURE FOR DYNAMICAL AND STATISTICAL EMISSIONS

In order to have an overall view of the kinematical properties of emitted particles and fragments, it is instructive to plot the invariant cross section contours $d^2\sigma/v_\perp dv_\perp dv_\parallel$ in a $v_\perp$ vs $v_\parallel$ plot.

In Fig. 2 such plots, in the center-of-mass (c.m.) reference frame, are shown for protons and $\alpha$ particles and for several $E_{trans12}$ bins.

The binary source behavior is easily recognized for bins 1–4. For more violent collisions, the separation between the two sources is not so clear and the last bin can correspond to fusionlike events. Now, an interesting observation can be drawn from these figures: When two sources are clearly resolved, all $\alpha$ particles cannot be attributed to a statistical sequential decay since they would lie uniformly on circles centered around the recoil velocities. Instead, a larger abundance of particles is observed in between the two sources (see also [16]). This ''excess'' emission can be understood in at least two ways: They could either come from the first moments of the reaction and correspond to preequilibrium effects or come from a later stage of the reaction and correspond to various scenarios of the ''rupture of the neck.'' The two mechanisms probably contribute to the observed ''excess'' emission and there is a continuous evolution between them.

In the latter case, the binary system is dynamically strongly deformed, the ''neck'' region being either released (neck emission) or attached to one of the outgoing partners,

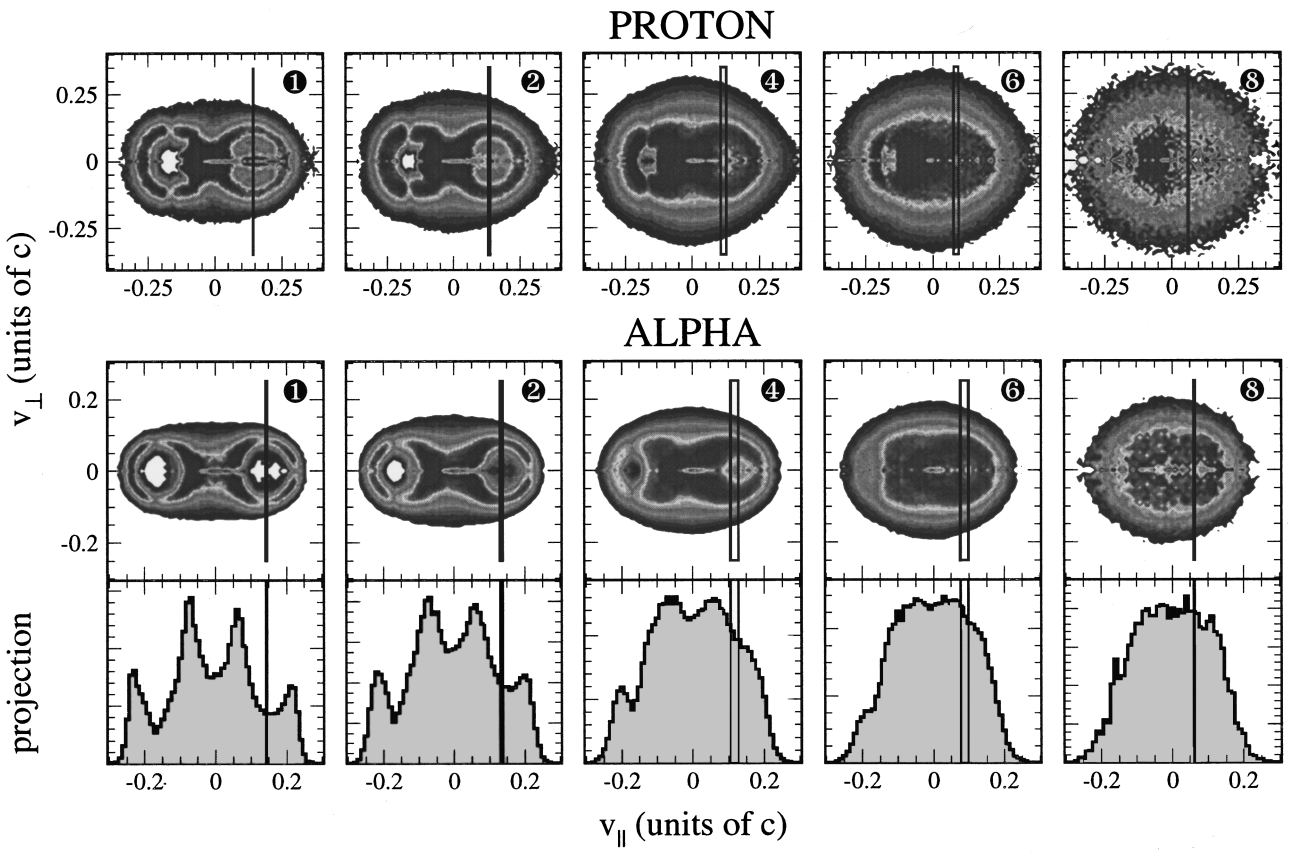


FIG. 2. Invariant c.m. velocity plots for protons (upper row) and $\alpha$ particles (lower row) for specified $E_{trans12}$ bins. The right and left sides of the rectangles superimposed on the velocity plots correspond to the source velocities obtained with the use of methods I and II, respectively (see text). The presented projections refer to $\alpha$ particle plots.

which is hence deformed beyond a pseudo saddle point, leading to a fast dynamical breakup. The memory of the partner direction is kept if the emission time is smaller than a few times $10^{-22}$ s, for an angular momentum in the range $(50–100)\hbar$. A kinematical difference between these two processes can be found in velocity distributions relatively to the main sources. In the case of a pure ''neck'' emission (two main sources + neck), the corresponding products are likely to be at rest in the c.m. frame. Such a contribution can be observed in Fig. 3 for several IMF's. In the case of fast dynamical emission, the relative kinetic energy between the detected fragment and its emission source is dominated by the corresponding Coulomb energy. Such a behavior is observed in Fig. 2 for $\alpha$ particles. It has also been clearly recognized in three-body events [8–10,12,22].

In the following sections, these fast nonequilibrated emissions will be referred to as ''dynamical'' or ''midvelocity'' emissions to distinguish them from the isotropic ''statistical'' emissions.

## V. QUANTITATIVE RESULTS

In order to quantify the importance of these dynamical emissions, the corresponding charge percentage is evaluated. For this purpose, one has to estimate the velocities of the two main sources, and to subtract the component which can be attributed to a sequential decay after complete equilibrium, and which is expected to lead to a forward-backward symmetrical emission in the source frame. Here, the difficulty is to determine properly the velocities of the two main sources.

We performed all the analysis on the QP side (positive c.m. velocities) for which detection efficiency was the best. Since the system is almost symmetric, the results can be easily extrapolated to the whole system. It should be stressed here that this analysis was applied to ensembles of events and thus, as a statistical analysis, it gives as results average numbers.

For the peripheral events (bins 1–4) for which the total charge detected is greater than that of the projectile, the velocity of the heaviest fragment on the PLF side can be regarded as the velocity of the quasiprojectile source (QPS). We have tested for each $E_{trans12}$ bin that the most probable velocities of these heaviest fragments are consistent with the apparent centers of the Coulomb rings observed in Figs. 2 and 3 for LCP's and IMF's. This observation can justify the assignment of these values of velocities to the QPS. However, it is necessary to stress that this method may lead to an overestimation because, as the fast sequential decay exhibits an angular anisotropy, the heaviest fragment is generally pushed in the forward direction in the QPS frame. Similarly, the anisotropy of $\alpha$ or IMF emission (Figs. 2 and 3) induces a shift of the invariant cross section isocontours.

For these reasons, besides the above method (labeled ''method I'' later on), we also utilized another method based on the thrust analysis [23,22] (''method II'') to extract the QPS and quasitarget source (QTS) velocities. This method is

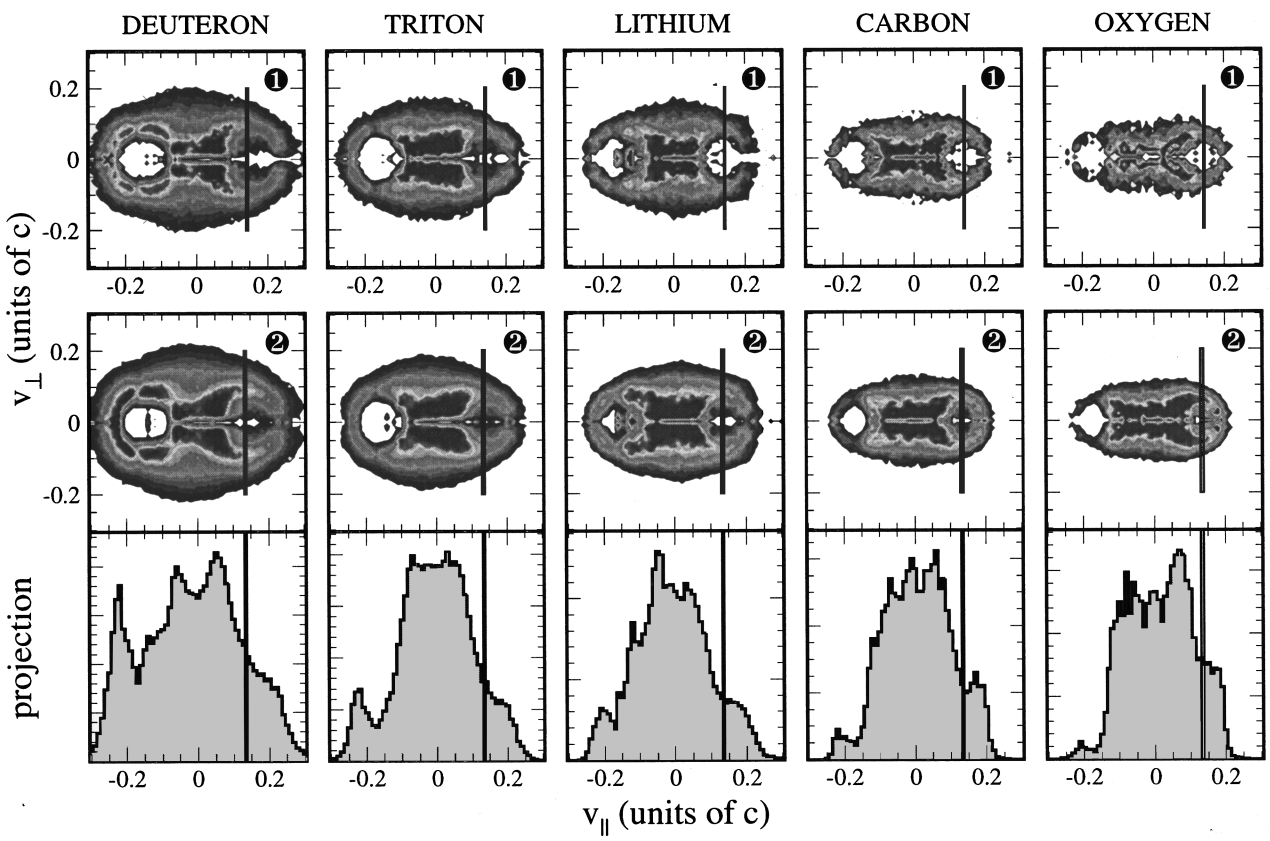


FIG. 3. Invariant c.m. velocity plots for deuteron, triton, lithium, carbon, and oxygen fragments detected in the most peripheral collisions (upper row, bin 1; and lower row, bin 2 of $E_{trans12}$). The right and left sides of the rectangles correspond to the source velocities obtained with the use of methods I and II, respectively (see text). The presented projections refer to the plots for the second bin.

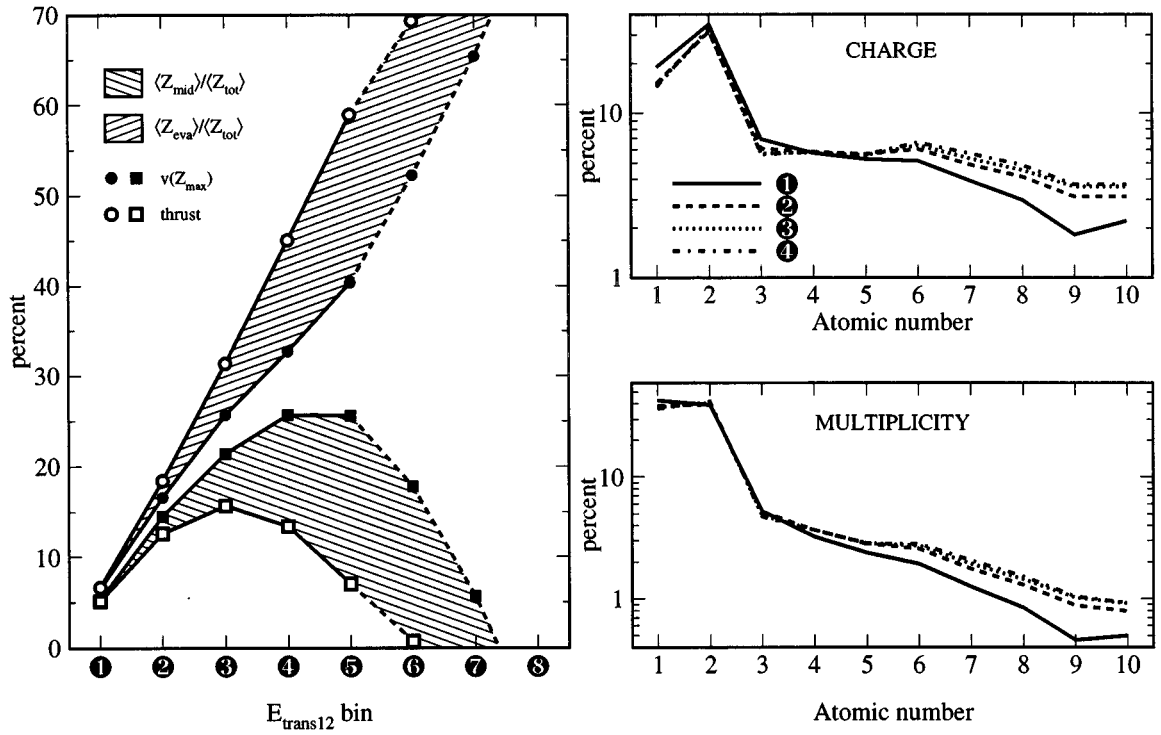


FIG. 4. Left panel: percentage of charge contained in the ''dynamical'' midvelocity component, the shaded area bounded by squares, and the percentage of charge coming from statistical emission, the shaded area bounded by circles. The solid and open symbols correspond to methods I and II, respectively. Upper right panel: the percentage of charge in the dynamical component coming from the fragments of a given $Z$ number ($Z$ from 1 to 10) for the $E_{trans12}$ bins 1–4. Lower right panel: same, but for the multiplicity. The right panels were obtained with the use of method I alone.

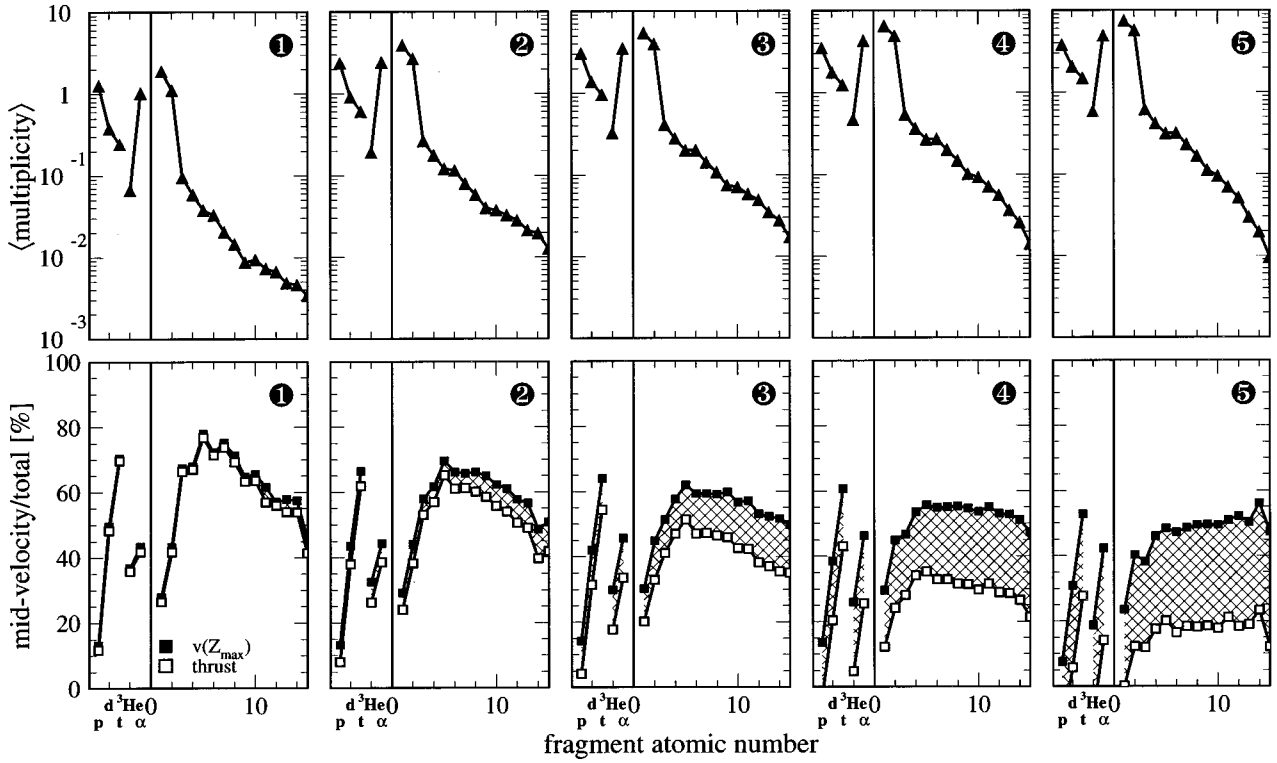


FIG. 5. Upper row: mean multiplicities of $p$, $d$, $t$, $^3$He, $\alpha$ and fragments with $Z \leqslant 15$ detected in the forward c.m. hemisphere for the first five $E_{trans12}$ bins. Lower row: contribution of the specified above fragments to the midvelocity component. The solid and open squares correspond to methods I and II, respectively.

well suited for complete events, for which the whole available charge has been detected. We extend it to events for which the targetlike residue has not been detected, but reconstructed from mass and momentum conservation laws. In the thrust analysis, one looks for the best way of attributing all the fragments ($Z \geqslant 3$) of an event to two sources by maximizing the quantity

$$T = \frac{\left|\sum \vec{p}_i\right| + \left|\sum \vec{p}_j\right|}{\sum |\vec{p}_k|}.$$

In the numerator, each summation includes fragments which have been attributed to a definite source. The denominator is simply a scaling factor. This method is fully correct if only two sources are involved in the selected events. It leads to underestimated values for the QPS if some neck emission occurs, since neck particles are included in the sharing between the two main sources.

Thus in the following analysis we utilize both the above methods and treat them as two extremes. The right and left sides of the rectangles superimposed on the velocity plots in Figs. 2 and 3 correspond to the source velocities obtained with the use of methods I and II, respectively.

Having defined the source velocities, it is now possible to estimate the size of the midvelocity (dynamical) component. It was done by doubling the yield of particles and fragments with velocities greater than the QPS velocity and subtracting it from the total yield in the forward c.m. hemisphere.

The results [24] are visualized in Fig. 4. Left part of this figure presents the percentage of charge coming from dynamical emissions—the shaded area bounded by square symbols—and the percentage of charge coming from statistical emission—the shaded area bounded by circles. The solid and open symbols correspond to methods I and II, respectively. The width of the bands reflects the sensitivity of the method in measuring the size of the dynamical component on the source velocity. As can be seen, the percentage of dynamically emitted charge reaches from 12% to 25%, depending on the assumption used to calculate the QPS velocity. Thus it represents a sizable fraction of LCP's and IMF's emitted during the collision.

It should be stressed, however, that the results above bins 4 and 5 (the dashed lines in Fig. 4) should be taken with some care (and in particular the existence of the maximum in the midvelocity/total ratio), since they present the results of the extrapolation of the subtraction method above the range of its applicability. Indeed, for small relative velocities between QPS and QTS, the method tends to overestimate the isotropic contribution associated with the two main sources, and thus underestimates the midvelocity component. For the most central collisions, this can even lead to negative values.

The right panels of Fig. 4 address the question concerning the composition of the dynamical component. The four lines correspond to the $E_{trans12}$ bins 1–4 and they represent the contribution of fragments with a given $Z$ number to the charge (upper panel) and multiplicity (lower panel) of the dynamical component. As can be seen from the upper panel the charge of the midvelocity particles comes mainly from LCP's [(30–35)% from helium isotopes and (15–20)% from

hydrogen isotopes], the rest of the charge [(45–55)%] comes from the IMF's. In the case of multiplicities these contributions are, respectively, 40% for helium isotopes, (35–40)% for hydrogen isotopes, and (20–25)% for IMF's. Thus the dynamical component consists mainly of LCP's, but IMF's represent a sizable fraction of charge and multiplicity, and their importance increases with the increasing centrality of the collisions.

The above signatures of strong dynamical effects are also clearly seen in Fig. 5 in which the lower row presents, for five $E_{trans12}$ bins, the mean percentage of various particles or fragments, which are attributed to dynamical component in methods I and II (solid and open squares, respectively).

As can be seen up to (60–80)% of light IMF's ($3 \leqslant Z \leqslant 6$) detected in the most peripheral (bins 1 and 2) collisions originate from the midvelocity region. Also a very large fraction of tritons [(65–70)%] comes from this zone, which may indicate that the midvelocity emission systematically favors the neutron-rich isotopes. The upper row of this figure presents the mean multiplicities per event in the forward c.m. hemisphere for various LCP's and IMF's. It indicates the relative contributions of the emission of various products. If one integrates the multiplicity distribution for IMF's and takes into account the dynamical component, one ends up with one to two IMF's emitted dynamically per event for bins 2–4 (after extrapolating the value to the whole, i.e., projectile + target, system). This value is greater than or comparable to the mean number of statistically emitted IMF's in this region of impact parameters. Thus the dynamical emissions of IMF's in peripheral and semicentral collisions for the system under consideration is not at all an exotic process; moreover, it seems to represent the main source of IMF's for the impact parameters considered.

## VI. COMPARISON WITH DYNAMICAL MODELS

Reliable information about the reaction mechanisms involved in heavy-ion collisions at intermediate energies can be obtained in the framework of one-body transport theories. The Landau-Vlasov [(LV), Boltzmann-Uehling-Uhlenbeck (BUU), or Boltzmann-Northeim-Vlasov (BNV)] transport equation, which describes the time evolution of the nucleon one-body distribution function in phase space, $f(\vec{r},\vec{p},t)$, provides a generally good average description of the dissipative mechanisms occurring all along the interaction between the two colliding nuclei. Depending on entrance channel properties, namely, the impact parameter, the beam energy, and the mass asymmetry, different outcoming channels, ranging from the formation of only one composite nuclear source, in the case of violent collisions, up to deep-inelastic-like processes, for peripheral reactions, are observed [25,7].

In such a context, in this section we will try to get a deeper insight into the reaction mechanisms which could be responsible for the midvelocity emission observed in Xe + Sn at 50 MeV/nucleon. As mentioned in the Introduction, a possible explanation for the presence of matter in this velocity region could be, in fact, the dynamical formation of an elongated dinuclear system, in the case of semicentral reactions, which breaks into more than two primary fragments, a QP, a QT, and a composite source which originates from the overlapping region (the neck zone).

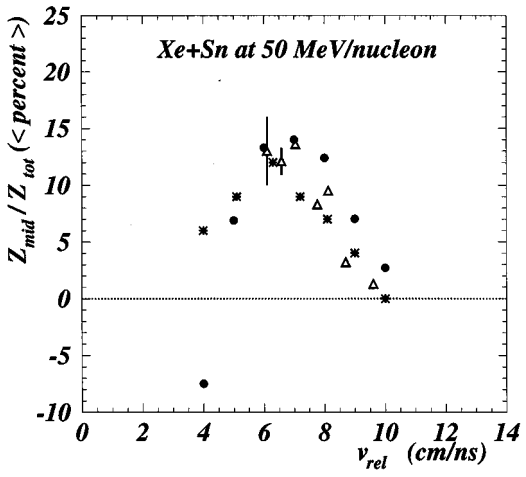


FIG. 6. Midvelocity emission (in %) as a function of the relative velocity between the QPS and the QTS. Solid circles correspond to the experimental data, triangles to Landau-Vlasov calculations, and stars to stochastic mean-field calculations.

In one-body transport theories [26] the time evolution of the distribution function $f(\vec{r},\vec{p},t)$ is ruled by the action of a mean-field potential, together with the effect of a Pauli-blocked collision term, according to the equation

$$\frac{\partial f(\vec{r},\vec{p},t)}{\partial t} + \{f(\vec{r},\vec{p},t),H\} = I_{\text{coll}}(f(\vec{r},\vec{p},t)), \qquad (1)$$

where $\{,\}$ stands for the Poisson brackets, $H$ is the self-consistent one-body Hamiltonian, and $I_{\text{coll}}$ is the Uehling-Uhlenbeck collision term. Based on previous studies on collective flow [27], the momentum-dependent Gogny interaction D1G1 [28] and the energy-dependent free nucleon-nucleon cross section have been used in our calculations. These two features act together and their relative contribution is crucial for the evolution of the colliding system.

Simulations have been done for impact parameters between 2 and 11 fm. Equation (1) is solved using the test particle method. We have used 45 test particles per nucleon. The calculations have been stopped at 300 fm/$c$ and Coulomb trajectory calculations have been performed, which allow us to obtain the asymptotic distribution of the pseudoparticles in $\vec{p}$ space. Over the whole range of impact parameters studied, a binary mechanism is observed. In such a case the pseudoparticles appear located in two main regions in $\vec{p}$ space, which can be associated, respectively, with the QP and the QT. However, it is possible to recognize also a component located around the center-of-mass velocity region. In order to extract this component, we have adopted a prescription as close as possible to the experimental analysis, extracting the QPS and QTS velocities by considering a method closely connected to the thrust analysis (method II). When using ''method I'' to determine the source velocities, we obtain the same kind of agreement between the data and the calculation. Once the velocity of the two main sources has been determined, the midvelocity component is extracted following the procedure presented in Sec. V. In Fig. 6, the midvelocity emission ($\langle$percent$\rangle$) has been plotted as a func-

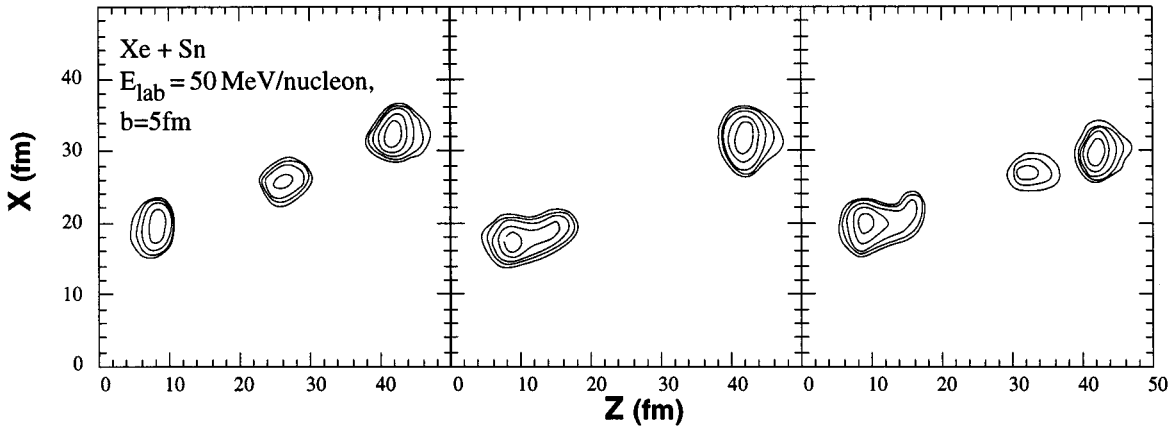


FIG. 7. Density contour plots in the coordinate space for three sample events obtained within the framework of the stochastic mean-field calculation. The events are associated with $b=5$ fm and measured after 260 fm/$c$. See the text for a detailed explanation.

tion of the relative velocity between the QPS and QTS ($V_{\rm rel}$). This allows us to make a direct comparison between the calculated and the average experimental values. Solid circles correspond to experimental measurements and open triangles to one-body model calculations. Error bars in the model calculation account for different impact parameters giving the same $V_{\rm rel}$.

As can be seen, the theoretical estimation is quite close to the experimental one. The maxima of both distributions are very close and are located around the same $V_{\rm rel}$ (6.5 cm/ns). This corresponds in our simulations to a maximum of the midvelocity emission at impact parameters between 5 and 6 fm.

In addition to that, the shape of the distribution is also quite well reproduced for $V_{\rm rel}$ greater than 6 cm/ns.

This good agreement gives us some confidence to continue our investigation and try to extract more information about the origin of the midvelocity component obtained in the calculations. By looking at the distribution of the pseudoparticles in coordinate space, one can actually observe the formation of an elongated dinuclear system, which breaks into pieces after $\approx 150$ fm/$c$. The particles coming from the neck region, after the breakup, surely contribute to the midvelocity component extracted above. However, in order to complete the analysis, we have evaluated also the particles emitted before the neck rupture. These particles have been tagged in the calculations, so that their contribution to the midvelocity emission can be recognized at the end of the calculations. We find that up to 50% of the midvelocity emission comes from early emitted particles.

While the LV calculations presented above provide a good estimation of the average contribution related to the midvelocity particle emission, a study of the fluctuations involved in the dynamics of the neck emission can be achieved in the framework of stochastic mean-field calculations. Indeed, at sufficiently high beam energy, an analysis of the dynamical evolution of the neck region puts in evidence the possibility for this part of the system to reach, after the initial collisional shock, low values of the density and, hence, to encounter volume instabilities. Shape instabilities could also likely develop in this overlapping zone. From the experimental point of view, a detectable consequence of the occurrence of instabilities should be the possibility to have a ''direct'' dynamical component in the IMF emission, as well as the observation of large variances for the observables related to QPS and QTS.

The effects due to the development of instabilities in the mean-field dynamics can be accounted for by considering a stochastic extension of Eq. (1). The system is still described through its one-body distribution function, but this function may experience a stochastic evolution in response to the action of a fluctuation source term, which is related to the random nature of the thermal motion of the nucleons. This means that a stochastic part is added to the collision integral $\delta I_{\rm coll}$ on the right-hand side (RHS) of Eq. (1). In this way, the system is described by an ensemble of fluctuating one-body distribution functions $\{f^n\}$. In the following calculations a Skyrme-like parametrization is used for the description of the mean-field potential, which gives a ''soft'' equation of state, with a compressibility modulus $K=200$ MeV. The procedure used for the introduction of fluctuations into the dynamical evolution is explained in Ref. [29].

Calculations have been done for impact parameters ranging from 2 to 11 fm, as in the case of the LV calculations. Indeed the formation of a ''neck'' region is observed, by looking at the spatial density distribution, in this impact parameter range. A set of ten events has been considered for each impact parameter. For a given impact parameter, the calculations show that several configurations can develop in the neck region. As an example, Fig. 7 shows the density contour plots in coordinate space for three events associated with $b=5$ fm, at 260 fm/$c$. It can be seen that a quite different evolution is possible for the neck region: IMF's may directly originate from the overlapping zone (event 1). The neck region may be reabsorbed by one of the spectators (or both), leading to the formation of deformed QP or QT (event 2), which may break up, most likely, through a fast-fission mechanism; both mechanisms present in events 1 and 2 may coexist (event 3).

For each event the same analysis performed in the experimental case (and recalled above) can be repeated, in order to extract the midvelocity component. The average value of the charge associated with the component extracted in this way is presented in Fig. 6 (in percent) using black stars. It should be noticed that only the particles evaporated from the three regions have been considered in this analysis; i.e., the ''pre-

equilibrium'' emission has been removed here. The large discrepancy observed at low $V_{\rm rel}$ is probably coming from the difficulty to extend our analysis to low impact parameters. In this case the three sources are not clearly separated in **p** space, and so the value extracted for the midrapidity component depends very much on the estimation of the relative velocity $V_{\rm rel}$. Also, for the most dissipative collisions, when fluctuations are expected to play a more important role, a larger number of fluctuating events should be considered. However, a detailed analysis of fluctuations, which is quite computer demanding, goes beyond the aim of the present article.

In conclusion, transport theories seem to describe well the mechanism responsible for the midvelocity emission observed experimentally. This component is essentially related first to prompt emission and, at a later time in the reaction, to the emission from the ''neck'' matter which develops in the overlapping zone. A question that could be addressed is the sensitivity of the calculated midvelocity component to the main ingredients of the model, namely, the nuclear compressibility and the nucleon-nucleon cross section. In particular, the midvelocity emission is expected to be strongly correlated to the amount of *n*-*n* collisions. In the calculations this can be easily modified by changing the *n*-*n* cross section $\sigma_{nn}$. This work is presently in progress.

## VII. SUMMARY AND CONCLUSIONS

The present analysis, valid for about (80–90)% of the total measured cross section, indicates that dynamical effects are important in peripheral and intermediate impact parameter collisions at 50 MeV/nucleon. It shows effects that differ distinctly both from the lower-energy deep-inelastic reaction mechanism and from the high-energy spectator/participant model: These results belong therefore to the transition region between these two extreme scenarios.

These dynamical emissions, which have been statistically separated from what is supposed to be the isotropic (in the emitting reference frame) statistical emissions, seem to come from two different processes: prompt emitted particles (preequilibrium ?) and ''neck''-related emissions of particles and IMF's.

Together, these contributions represent up to (12–25)% of the total charge for at least 50% of the measured reaction cross section. This is almost as much as is obtained from isotropic statistical emissions. Up to (45–60)% of the IMF's produced in peripheral collisions (bins 1–4, 86% of the measured $\sigma_{\rm tot}$) originate from the intermediate velocity region: This is therefore a first order effect which should be considered when studying, for example, the nature of these emissions [30]. When mass resolution is obtained, midvelocity emissions systematically favor the neutron-rich isotopes. These observations are very similar to those published by Dempsey *et al.* [17] for very similar systems.

For the first time, the amount of charge and mass related to these dynamical emissions has been measured as a function of the particle transverse energy, giving some insight into the impact parameter dependence of these effects.

One of the more important questions that these results raise concerns the nature of the dissipative mechanism. At low energy, a mechanism based on the exchange of nucleons across the ''window'' between the nuclei during the collision is invoked to explain the kinetic energy loss and the heating of the nuclei. At very high energy, almost no kinetic energy loss is suffered for the spectators (which are heated because of modification of the surface and of ''hole punching'' in the Fermi sea) whereas the participants are highly excited, independently of the impact parameter for symmetric systems. In the present energy domain and for these symmetric systems the mechanism could be more complicated and should be compared to the dynamical models that are used to study these collisions: BUU, QMD, etc.

Calculations with Landau-Vlasov codes reproduce the amount of dynamical emissions as a function of the relative velocity between the outgoing nuclei. A study including fluctuations gives very interesting insight into the variety of scenarios that are related to the so-called ''neck emissions'' or ''dynamical fission.'' Whether these encouraging results imply that the dissipative mechanisms are correctly reproduced and explained as a function of impact parameter is the challenge of future experimental and theoretical studies.

## ACKNOWLEDGMENTS

J.L. wishes to thank the members of the INDRA Collaboration at the IPN Orsay for their very warm hospitality. He thanks the Ministère de l'Enseignement Supérieur et de la Recherche for financial support.

[1] B. Borderie, M. Montoya, M. F. Rivet, D. Jouan, C. Cabot, H. Fuchs, D. Gardes, H. Gauvin, D. Jacquet, F. Monnet, and F. Hanappe, Phys. Lett. B **205**, 26 (1988); M. F. Rivet, B. Borderie, P. Box, M. Dakowski, C. Cabot, D. Gardes, D. Jouan, G. Mamane, X. Tarrago, H. Utsunomiya, Y. El Masri, F. Hanappe, F. Sébille, and F. Haddad, in Proceedings of the International Winter Meeting on Nuclear Physics, Bormio, 1993, edited by I. Iozi, p. 92.

[2] J. Péter, S. C. Jeong, J. C. Angélique, G. Auger, G. Bizard, R. Brou, A. Buta, C. Cabot, Y. Cassagnou, E. Crema, D. Cussol, D. Durand, Y. El Masri, P. Eudes, Z. Y. He, A. Kerambrun, C. Lebrun, R. Legrain, J. P. Patry, A. Péghaire, R. Régimbart, E. Rosato, F. Saint-Laurent, J. C. Steckmeyer, B. Tamain, and E. Vient, Nucl. Phys. **A593**, 95 (1995).

[3] J. C. Steckmeyer, A. Kerambrun, J. C. Angélique, G. Auger, G. Bizard, R. Brou, C. Cabot, E. Crema, D. Cussol, D. Durand, Y. El Masri, P. Eudes, M. Gonin, K. Hagel, Z. Y. He, S. C. Jeong, C. Lebrun, J. P. Patry, A. Péghaire, J. Péter, R. Régimbart, E. Rosato, F. Saint-Laurent, B. Tamain, E. Vient, and R. Wada, Report No. LPCC 95-13, 1995.

[4] R. Bougault, J. F. Lecolley, M. Aboufirassi, A. Badala, B. Bilwes, R. Brou, J. Colin, F. Cosmo, D. Durand, J. Galin, A. Genoux-Lubain, D. Guerreau, D. Horn, D. Jacquet, J. L. Laville, C. Le Brun, F. Lefebvres, O. Lopez, M. Louvel, M. Mahi, M. Morjean, C. Paulot, A. Péghaire, G. Rudolf, F. Scheibling, J. C. Steckmeyer, L. Stuttgé, S. Tomasevic, and B.

Tamain, Nucl. Phys. **A587**, 499 (1995).

[5] V. Métivier, B. Tamain, G. Auger, C. O. Bacri, A. Benkirane, J. Benlliure, B. Berthier, B. Borderie, R. Bougalut, P. Box, R. Brou, Y. Cassagnou, J. L. Charvet, A. Chbihi, J. Colin, D. Cussol, R. Dayras, E. De Filippo, A. Demeyer, D. Durand, P. Ecomard, P. Eudes, A. Genoux-Lubain, D. Gourio, D. Guinet, R. Laforest, L. Lakehal-Ayat, P. Lautesse, J. L. Laville, L. Lebreton, C. Le Brun, J. F. Lecolley, A. Le Fèvre, R. Legrain, O. Lopez, M. Louvel, M. Mahi, N. Marie, T. Nakagawa, L. Nalpas, A. Ouatizerga, M. Parlog, J. Péter, E. Plagnol, E. Pollacco, A. Rahmani, R. Régimbart, T. Reposeur, M. F. Rivet, E. Rosato, F. Saint-Laurent, M. Squalli, J. C. Steckmeyer, L. Tassan-Got, E. Vient, C. Volant, J. P. Wieleczko, A. Wieloch, and K. Yusa-Nakagawa, in Proceedings of the ACS Nuclear Chemistry Symposium, Anaheim, CA, 1995.

[6] M. F. Rivet, B. Borderie, C. Grégoire, D. Jouan, and B. Remaud, Phys. Lett. B **215**, 55 (1988); M. Colonna, M. Di Toro, V. Latora, and A. Smerzi, Prog. Part. Nucl. Phys. **30**, 17 (1992); L. Sobotka, Phys. Rev. C **50**, R1272 (1994); M. Colonna, M. Di Toro, and A. Guarnera, Nucl. Phys. **A589**, 160 (1995).

[7] F. Haddad, B. Borderie, V. De La Mota, M. F. Rivet, F. Sebille, and B. Jouault, Z. Phys. A **354**, 321 (1996).

[8] P. Glässel, D. v. Harrach, H. J. Specht, and L. Grodzins, Z. Phys. A **310**, 189 (1983).

[9] G. Casini, P. G. Bizzeti, P. R. Maurenzig, A. Olmi, A. A. Stefanini, J. P. Wessels, R. J. Charity, R. Freifelder, A. Gobbi, N. Herrmann, K. D. Hildenbrand, and H. Stelzer, Phys. Rev. Lett. **71**, 2567 (1993).

[10] L. Stuttgé, J. C. Adloff, B. Bilwes, R. Bilwes, F. Cosmo, M. Glaser, G. Rudolf, F. Scheibling, R. Bougalut, J. Colin, F. Delaunay, A. Genoux-Lubain, D. Horn, C. Le Brun, J. F. Lecolley, M. Louvel, J. C. Steckmeyer, and J. L. Ferrero, Nucl. Phys. **A539**, 511 (1992).

[11] R. Wada, M. Gonin, M. Gui, K. Hagel, Y. Lou, D. Utley, B. Xiao, D. Miller, J. B. Natowitz, D. Fabris, G. Nebbia, R. Zanon, B. Chambon, B. Cheynis, A. Demeyer, D. Drain, D. Guinet, X. C. Hu, C. Pastor, K. Zaid, J. Alarja, R. Bertholet, A. Giorni, A. Lleres, C. Morland, P. Stassi, L. Schussler, B. Viano, and P. Gonthier, Nucl. Phys. **A548**, 471 (1992).

[12] J. F. Lecolley, L. Stuttgé, M. Aboufirassi, B. Bilwes, R. Bougault, R. Brou, F. Cosmo, J. Colin, D. Durand, J. Galin, A. Genoux-Lubain, D. Guerreau, D. Horn, D. Jacquet, J. L. Laville, F. Lefebvres, C. Le Brun, O. Lopez, M. Louvel, M. Mahi, C. Meslin, M. Morjean, A. Péghaire, G. Rudolf, F. Scheibling, J. C. Steckmeyer, B. Tamain, and S. Tomasevic, Phys. Lett. B **354**, 202 (1995).

[13] C. P. Montoya, W. G. Lynch, D. R. Bowman, G. F. Peaslee, N. Carlin, R. T. De Souza, C. K. Gelbke, W. G. Gong, Y. D. Kim, M. A. Lisa, L. Phair, M. B. Tsang, J. B. Webster, C. Williams, N. Colonna, K. Hanold, M. A. Mc Mahan, G. J. Wozniak, and L. G. Moretto, Phys. Rev. Lett. **73**, 3070 (1994).

[14] J. Tõke, B. Lott, S. P. Baldwin, B. M. Quednau, W. U. Schröder, L. G. Sobotka, J. Barreto, R. J. Charity, D. G. Sarantites, D. W. Stracener, and R. T. De Souza, Phys. Rev. Lett. **75**, 2920 (1995); J. Tõke, B. Lott, S. P. Baldwin, B. M. Quednau, W. U. Schröder, L. G. Sobotka, J. Barreto, R. J. Charity, L. Gallamore, D. G. Sarantites, D. W. Stracener, and R. T. De Souza, Nucl. Phys. **A583**, 519c (1995).

[15] W. Lynch, Nucl. Phys. **A583**, 471c (1995).

[16] J. E. Sauvestre, J. L. Charvet, R. Dayras, C. Volant, B. Berthier, R. Legrain, R. Lucas, E. C. Pollacco, E. De Filippo, G. Lanzanó, A. Pagano, C. Beck, and B. Djerroud, Phys. Lett. B **335**, 300 (1994).

[17] J. F. Dempsey, R. J. Charity, L. G. Sobotka, G. J. Kunde, S. Gaff, C. K. Gelbke, T. Glasmacher, M. J. Huang, R. C. Lemmon, W. G. Lynch, L. Manduci, L. Martin, M. B. Tsang, D. K. Agnihotri, B. Djerroud, W. U. Schröder, W. Skulski, J. Tõke, and W. A. Friedman, Phys. Rev. C **54**, 1700 (1996).

[18] J. Tõke, D. K. Agnihotri, S. P. Baldwin, B. Djerroud, B. Lott, B. M. Quednau, W. Skulski, W. U. Schröder, L. G. Sobotka, R. J. Charity, D. G. Sarantites, and R. T. de Souza, Phys. Rev. Lett. **77**, 3514 (1996).

[19] N. Ashgriz and J. Y. Poo, J. Fluid Mech. **221**, 183 (1990).

[20] J. Pouthas, B. Borderie, R. Dayras, E. Plagnol, M. F. Rivet, F. Saint-Laurent, J. C. Steckmeyer, G. Auger, C. O. Bacri, S. Barbey, A. Barbier, A. Benkirane, J. Benlliure, B. Berthier, E. Bougamont, P. Bourgault, P. Box, R. Bzyl, B. Cahan, Y. Cassagnou, D. Charlet, J. L. Charvet, A. Chbihi, T. Clerc, N. Copinet, D. Cussol, M. Engrand, J. M. Gautier, Y. Huguet, O. Jouniaux, J. L. Laville, P. Le Botlan, A. Leconte, R. Legrain, P. Lelong, M. Le Guay, L. Martina, C. Mazur, P. Mosrin, L. Olivier, J. P. Passerieux, S. Pierre, B. Piquet, E. Plaige, E. C. Pollacco, B. Raine, A. Richard, J. Ropert, C. Spitaels, L. Stab, D. Sznajderman, L. Tassan-Got, J. Tillier, M. Tripon, P. Vallerand, C. Volant, P. Volkov, J. P. Wieleczko, and G. Wittwer, Nucl. Instrum. Methods Phys. Res. A **357**, 418 (1995); J. Pouthas, A. Bertraut, B. Borderie, P. Bourgault, B. Cahan, G. Carles, D. Charlet, D. Cussol, R. Dayras, M. Engrand, O. Jouniaux, P. Le Botlan, A. Leconte, P. Lelong, L. Martina, P. Mosrin, L. Olivier, J. P. Passerieux, B. Piquet, E. Plagnol, E. Plaige, B. Raine, A. Richard, F. Saint-Laurent, C. Spitaels, J. Tillier, M. Tripon, P. Vallerand, P. Volkov, and G. Wittwer, *ibid.* **369**, 222 (1996).

[21] C. Cavata, M. Demoulins, J. Gosset, M.-C. Lemaire, D. L'Hôte, J. Poitou, and O. Valette, Phys. Rev. C **42**, 1760 (1990).

[22] V. Métivier, Ph.D. thesis, University of Caen (France), 1995.

[23] J. Cugnon and D. L'Hôte, Nucl. Phys. **A397**, 519 (1983).

[24] J. Łukasik, J. F. Lecolley, V. Métivier, E. Plagnol, B. Tamain, G. Auger, Ch. O. Bacri, J. Benlliure, B. Borderie, R. Bougault, R. Brou, J. L. Charvet, A. Chbihi, J. Colin, D. Cussol, R. Dayras, E. De Filippo, A. Demeyer, D. Durand, P. Ecomard, P. Eudes, D. Gourio, D. Guinet, R. Laforest, P. Lautesse, J. L. Laville, L. Lebreton, A. Le Fèvre, T. Lefort, R. Legrain, O. Lopez, M. Louvel, N. Marie, L. Nalpas, A. Ouatizerga, M. Parlog, J. Péter, A. Rahmani, T. Reposeur, M. F. Rivet, E. Rosato, F. Saint-Laurent, M. Squalli, J. C. Steckmeyer, L. Tassan-Got, E. Vient, C. Volant, and J. P. Wieleczko, in Proceedings of the International Winter Meeting on Nuclear Physics, Bormio, 1996, p. 36. The final results presented in this article differ slightly from those presented at the BORMIO'96 Winter Meeting on Nuclear Physics. The reason is that for the present results we utilize more accurate energy calibration. The discrepancies reflect the sensitivity of the method to this energy calibration.

[25] M. Colonna, N. Colonna, A. Bonasera, and M. Di Toro, Nucl. Phys. **A541**, 295 (1992).

[26] B. Remaud, C. Grégoire, F. Sébille, and P. Schuck, Nucl. Phys. **A488**, 423c (1988).

[27] F. Haddad, F. Sébille, M. Farine, P. Schuck, V. de la Mota, and B. Jouault, Phys. Rev. C **52**, 2013 (1995).

[28] J. Dechargé and D. Gogny, Phys. Rev. C **21**, 1568 (1980).
[29] M. Colonna and Ph. Chomaz, Phys. Rev. C **49**, 1908 (1994); M. Colonna, M. Di Toro, and A. Guarnera, Nucl. Phys. **A589**, 160 (1995).
[30] K. Tso, L. Phair, N. Colonna, W. Skulski, G. J. Wozniak, L. G. Moretto, D. R. Bowman, M. Chartier, C. K. Gelbke, W. G. Gong, W. C. Hsi, Y. D. Kim, M. A. Lisa, W. G. Lynch, G. F. Peaslee, C. Schwarz, R. T. De Souza, M. B. Tsang, and F. Zhou, Phys. Lett. B **361**, 25 (1995).